Half-Sarcomere Dynamics in Myofibrils during Activation and Relaxation Studied by Tracking Fluorescent Markers

Ivo A. Telley,* Jachen Denoth,* Edgar Stüssi,* Gabriele Pfitzer,† and Robert Stehle†
*Laboratory for Biomechanics, ETH Zurich Hönggerberg, 8093 Zürich, Switzerland; and †Institute of Vegetative Physiology, University of Cologne, 50931 Cologne, Germany

ABSTRACT To study the dynamics of individual half-sarcomeres in striated muscle contraction, myofibrils prepared from rabbit psoas muscle and left ventricles of guinea pig were immunostained with two conjugated antibody complexes consisting of a primary antibody against either α-actinin or myomesin and a secondary fluorescently labeled Fab-fragment. We simultaneously measured force kinetics and determined the positions of the Z-line and M-band signals by fluorescence video microscopy and sophisticated computer vision (tracking) algorithms. Upon calcium activation, sarcomeres and half-sarcomeres shortened nonuniformly. Shortening occurred first rapidly and exponentially during the force rise and then slowly during the force plateau. In psoas myofibrils, time-resolved displacements of the A-band in sarcomeres were observed, i.e., the two halves of individual sarcomeres behaved nonuniformly. Nonuniformity in length changes between the two halves of sarcomeres was comparable to that between two adjacent half-sarcomeres of neighboring sarcomeres. Sequential lengthening of half-sarcomeres was observed in cardiac myofibrils during the rapid phase of force relaxation. The independent dynamics of the halves in a sarcomere reveals the half-sarcomere as the functional unit rather than the structural unit, the sarcomere. The technique will facilitate the study of filament sliding within individual half-sarcomeres and the mechanics of intersegmental chemomechanical coupling in multisegmental striated muscles.

INTRODUCTION

The mechanical and kinetic characterization of contracting muscle is generally made in terms of the interaction between actin and myosin cross-bridges, assuming that these force-generating motors act independently and homogeneously along the muscle fiber. It is generally accepted that muscle shortening and lengthening is due to the actin and myosin filaments sliding past each other (1,2) and that cross-bridge kinetics is affected by the amount and speed of filament sliding (3–5). Strictly speaking, only those cross-bridges that are acting in a single half-sarcomere, with one-half of thick myosin filaments overlapping with the thin actin filaments, are similarly affected by the filament sliding in that particular half-sarcomere, a circumstance which leads to the theory of the functional unit half-sarcomere.

During myofibrillar contraction, many thousands of (half-)sarcomeres in series generate the same force while they shorten or lengthen. The sliding filament theory predicts that the half-sarcomere is an intrinsically unstable construction. Since active force decreases with decreasing actomyosin overlap (6), an initially lengthening half-sarcomere would loose force capacity progressively and lengthen even more, until a passive stabilizing structure (e.g., titin, desmin) bears the force. In fact, it was shown earlier by electron microscopy that displacements of the A-bands occur in activated muscle (7,8). Presumably one-half of the sarcomere might be stronger than the other half due to differences in the number of potential cross-bridge formations, thereby stretching the weak half-sarcomere, resulting in a displacement of the thick filaments in the sarcomere. However, the dynamics of such A-band shifts, and of half-sarcomeres in general, has never been measured. Several observations of overall variability in lengths of sarcomeres (nonuniformity) have been made using the laser diffraction technique (9,10) or by determining segmental fiber lengths (6,11–13). The Huxley 1957 formalism (14) predicts that the kinetics of cross-bridge turnover is greatly influenced by the velocity of sliding between myosin and actin filaments. A natural conclusion is that the kinetic processes along the fiber are also nonuniform as a consequence of the nonuniform sarcomere dynamics. A common argument has been that inhomogeneities in $[Ca^{2+}]$ are present which produce this nonuniform behavior, although this has never been further pursued. However, the measured force kinetics is an unknown convolution of these variable processes. How exactly muscle force is generated and influenced in such a highly dynamic and nonuniform system has not been answered so far, presumably because the dynamic state of each individual half-sarcomere has to be known. For a meticulous study of sarcomeric variability and the kinetics of muscle contraction, the aim is to determine the dynamics of single sarcomeres or, even better, half-sarcomeres in a controlled ionic, e.g., $[Ca^{2+}]$, $[P_i]$, and [ADP] environment.

In the past, individual sarcomere length (SL) measurement was accomplished in bright field and phase contrast video microscopy of single myofibrils by means of a (semiautomatic)

Submitted July 8, 2005, and accepted for publication September 19, 2005.

Address reprint requests to Dr. Robert Stehle, Institute of Physiology, University of Cologne, Robert-Koch-Strasse 39, D-50931 Köln, Germany. Tel.: 49-221-4786952; Fax: 49-221-4786965; E-mail: robert.stehle@uni-koeln.de; or Dr. Jachen Denoth, Laboratory for Biomechanics, ETH Zurich, ETH Hönggerberg, HCI E 357.1 CH-8093 Zürich, Switzerland. Tel.: 41-44-6336216; Fax: 41-44-6331124; E-mail: jdenoth@ethz.ch.

0006-3495/06/01/514/17 $2.00

doi: 10.1529/biophysj.105.070334

profile analysis of the A-band or I-band patterns (15–18). Since the center of mass determined in the profile analysis defines the structural boundaries of neither a sarcomere nor of a half-sarcomere, it is not a reliable detection for SL (see Fig. 1). Hence, it will not be possible to study the true dynamics of filament sliding in half-sarcomeres unless the structural boundaries of a half-sarcomere are properly detected by appropriate markers.

Here, we present a method in which we determined the dynamics of individual half-sarcomeres of a myofibril by tracking fluorescently stained boundary markers in digital video streams. The myofibril is the ideal model since it can be prepared such that the number of involved sarcomeres is typically 10–20. It allows reliable analysis of individual half-sarcomeres in reasonable time. In the experiments here, force recording and video microscopy were done simultaneously during tension development, and relaxation induced by rapid steps in $[Ca^{2+}]$. Fast equilibration with the surrounding medium is guaranteed by the short diffusion distance. In subsequent image processing of the videos, the marker positions were extracted and the distances of adjacent markers were calculated to obtain half sarcomere lengths (hSLs).

We used fluorescence immunostaining without fixation and a few minutes of incubation time. We chose α-actinin as marker protein for the localization of the Z-line boundary. It has been shown recently that staining this abundant protein produces large signals suitable for image processing (19). The second boundary is the M-band, a protein scaffold that connects thick filaments at the center of the A-band. Myomesin is an integral component of the M-band and present in all kinds of vertebrate striated muscle (20). Labeling these two proteins has the advantage that, besides being true boundary markers, the spatial distance between the location of actomyosin interaction and the dyes is maximal, reducing undesirable effects of the staining on cross-bridge function.

Determination of individual hSLs in digital video microscopy requires a computer vision framework for high-resolution position detection. For this we applied a region-based tracking algorithm first introduced by Danuser and colleagues for differential interference contrast (DIC) video microscopy (21). As mentioned there, the algorithm is not limited to DIC and can be applied to other imaging applications. The idea of region-based methods is to seek interframe correspondence for all pixels within a region of interest (ROI) and, therefore, match the texture of image regions from one frame to the next. It has the advantage that the redundancy is high and noise is effectively averaged, which makes it robust against low signal/noise ratio (SNR). Even with a weak SNR this procedure can achieve subpixel resolution, which is relevant in hSL measurement. With high numerical aperture digital light microscopes, the pixel coverage in object space can be set down to ~50 nm square using a charge-coupled device chip with a small physical pixel size (22). Yet, we want to measure SL changes of several nanometers with a low NA, long distance objective. Hence, a combination of digital

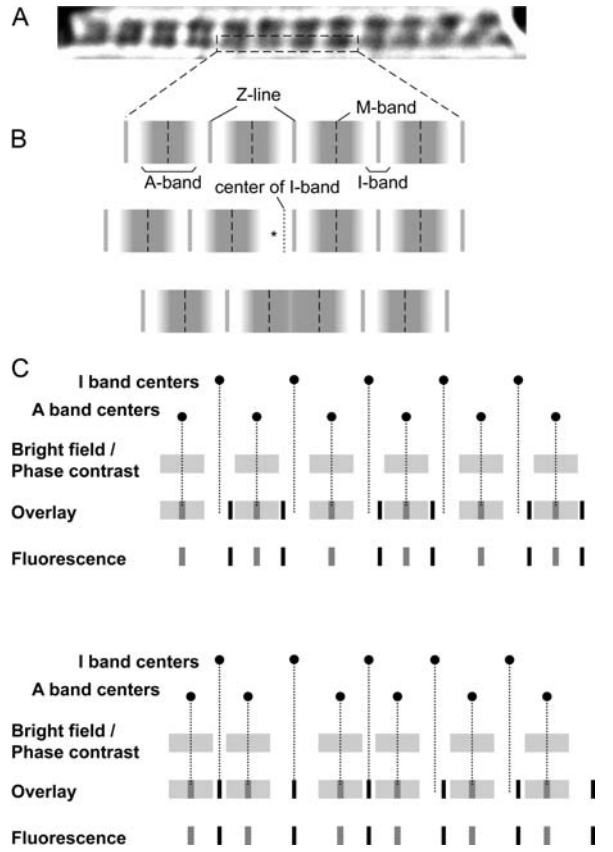

FIGURE 1 Limitations of a conventional profile analysis of sarcomeric band patterns. (*A*) Top: micrograph of a cardiac myofibril in phase contrast microscopy. (*B*) Schematic representations of band patterns. Dark bands represent the A-bands, with the invisible M-band in their center. Thick shaded lines represent the Z-line, which may not be detected properly at physiological SLs. If two adjacent half-sarcomeres become asymmetric in length, e.g., by filament sliding in a certain half-sarcomere (indicated by an asterisk), the center of the I-band determined in profile analysis no longer coincides with the Z-line, emphasized by the gap between the Z-line and the dashed line. Lengths of distinct sarcomeres bordered by Z-lines can then no longer be estimated correctly by analysis of the sarcomeric band pattern. Analysis of I-band centers would actually lead to the result that each of the two adjacent sarcomeres performed half of the length change, whereas with fluorescent markers lengths and length changes can be assigned correctly to half-sarcomeres. Bottom: during contraction, I-bands may diminish and A-bands come as close to each other such that they cannot be separated anymore (Rayleigh limit of resolution), whereas the distance between markers can still be evaluated even in short sarcomeres. (*C*) Information from sarcomeric band patterns and from sarcomeric boundary markers. Squares represent the A-bands observed in phase contrast or bright field microscopy. Solid and shaded lines indicate centers of Z-lines and M-bands detected by fluorescent markers. Top: if filament sliding is variable among, but symmetric in individual sarcomeres, variability in hSL or SLs (degree of half-sarcomere or sarcomere inhomogeneity) is underestimated from center fitting of A-band and/or I-bands. This is illustrated just for the extreme case of repetitive tandems of short and long sarcomeres. Bottom: the other extreme case in which all sarcomeres have similar length (Z–Z distance), but in which A-band shifts occur, which leads to an overestimate of SL variability, whereas hSL variability is still underestimated. Note that due to the unknown Z-line position, neither in the case of symmetrical nor asymmetrical (A-band shift) filament sliding can lengths of distinct sarcomeres and of half-sarcomeres be evaluated reliably from A-band and/or I-band centers.

video microscopy and high-resolution computer vision plays a key role in achieving the needs of accurate hSL detection. We present a method with which we obtain a temporal resolution of 10–50 ms and a resolution in terms of displacement of 5–20 nm, depending on the image quality.

MATERIALS AND METHODS

Myofibril preparation

Myofibrils were prepared from either skinned left ventricular trabeculae of the guinea pig or skinned strips from the rabbit psoas as previously described (18,23) except that animals were not anesthetized before sacrifice by cervical dislocation followed by exsanguination. All procedures were approved by the local animal care committee. Trabeculae or strips were dissected, then fixed isometrically with pins and skinned on ice for 4 h in skinning solution containing 5 mM K-phosphate, 5 mM Na-azide, 3 mM Mg-acetate, 5 mM K_2EGTA, 3 mM Na_2ATP (including 3 mM $MgCl_2$ and 6 mM KOH), 47 mM CrP, 2 mM DTT, 0.5 mM 4-(2-aminoethyl) benzenesulfonyl-fluoride HCl (AEBSF), 10 μM leupeptine, 10 μM antipaine, and 5 mg/ml aprotinine, adjusted to pH 6.8 at 20°C by Triton X-100 in a concentration of either 1% or 0.5% (v/v) for trabeculae or skeletal strips, respectively. After skinning, the solution was replaced by an identical one without Triton in which both preparations were stored up to 3 days at 4°C. Myofibrils were prepared immediately before an experiment by homogenization at 4°C in the same solution for 4–8 s at 12,000 rpm with a blender (Ultra-Turrax, IKA-Labortechnik, Staufen, Germany) and filtering the homogenate through 22 μm polypropylene meshes to remove aggregates of overcontracted myofibrils and large bundles.

Immunostaining and fluorescent dyes

A monoclonal anti-α-actinin Ab (mouse IgG1 isotype, clone EA-53, Sigma, Taufkirchen, Germany) was used as primary antibody (1:1000 v/v) for the localization of sarcomeric α-actinin in the Z-line. A monoclonal anti-myomesin Ab (mouse IgG1 isotype, clone B4) (24) was used as primary antibody (1:20 v/v) for the staining of all domains of myomesin localized in the M-band. For mechanical experiments, these two unlabeled antibodies were conjugated in the same aliquot with labeled (Alexa Fluor 488, Molecular Probes, Eugene, OR; Abs/Em: 495/519 nm) IgG Fab fragments (1:3 v/v) in a complex formation before the incubation of the samples (ZENON™ mouse IgG labeling kit, Invitrogen, Karlsruhe, Germany). Before staining, 3% (v/v) normal goat serum (NGS) was added to the myofibrillar suspension to block nonspecific binding sites. Samples were not chemically fixed for immunostaining. Total incubation time of the myofibrils with both antibody complexes was 10 min. A small droplet of the incubate was then diluted 1:50 in the relaxing solution filled into the trough of the apparatus (see below).

Apparatus

Besides some modifications described below, the apparatus we used was described earlier (18). All manipulators holding the thermostated trough, the microtools, and measurement instruments were mounted on a rigid stage of an Olympus IX-70 inverted microscope. The objective used in the experiments was either a 60×/0.70 Ph2 (LCPlanFl, Olympus) dry type with long working distance and cover glass correction cap (CAP-G 0.5 ± 0.5) or a 60×/1.2 W (UplanSApo, Olympus, Hamburg, Germany) water immersion type. The water immersion lens was cooled to the experimental temperature. The 1.5× magnification lens which is built in the IX-70 microscope was used for further image magnification. Epifluorescence microscopy was enabled via a mercury arc (HBO) lamp and a filter set (U-WIBA, Olympus) for blue excitation (excitation: BP460–490/beam split: DM505/emission filter: BA515–550). Experiments were conducted at 10°C. Small bundles containing one to three myofibrils were mounted in relaxing solution (see below) between the tips of a length-driving tungsten needle and an atomic force cantilever (Nanoprobe FESP type, compliance 0.25–0.5 μm/μN, resonant frequency in experimental solution 25–30 kHz) which had been coated with a mixture of nitrocellulose and a silicone adhesive. Before Ca^{2+} activation, mean slack SL and myofibrillar diameter were determined and then bundles were stretched in relaxing solution to a SL of 2.25–2.35 μm (cardiac) and 2.35–2.45 μm (psoas). These mounting and measurement steps were done in either phase contrast or bright field microscopy using a ultraviolet-blocking filter and a Yellow Filter (LC39 and Y52, Konica Minolta, Unterfoehring, Germany) to minimize photobleaching. Bundles were then Ca^{2+} activated and relaxed by rapidly translating the interface between two continuously flowing, laminar streams of solutions applied to the myofibril by a two-barrel micropipette. The force signal was obtained by reflection of a laser beam microfocused onto the back of the cantilever. During force recording, fluorescence patterns were recorded by digital video microscopy with a charge-coupled device camera (12 bit analog-digital converter). We used a slower camera (model ORCA-ER) and a faster camera (model C8800-01C), both from Hamamatsu Photonics (Herrsching, Germany), which had a physical pixel size of 6.45 μm square (image resolution: 71.7 nm/pixel) and 8 μm square (image resolution: 88.9 nm/pixel), respectively. With a Rayleigh resolution of 452 nm, the acquisition oversampling was ~6 for the ORCA-ER and ~5 for the C8800-01C.

Experimental solutions

Compared to our experimental solutions used in previous studies (18,23) and in some initial experiments for this study, we added 30 mM glutathione and increased the [DTT] from 2 mM to 30 mM. This greatly (5×) reduced the rundown in force observed in subsequent activation cycles of stained myofibrils during being exposed to the fluorescence exciting light. A further observed effect of the exciting light on stained myofibrils was an increase in passive force during subsequent experiments. This effect was completely abolished by adding the high [DTT] and the glutathione. Thus, we used here relaxing and activating solutions consisting of 10 mM imidazole, 3 mM K_4Cl_2EGTA (relaxing solution) or 3 mM $CaCl_2K_4$EGTA (activating), 1 mM Na_2MgATP, 3 mM $MgCl_2$, 37.7 mM Na_2CP, 30mM K-glutathione, and 30 mM DTT, adjusted to pH 7.0 at 10°C and consisting of a final formal ionic strength (μ) of 170 mM. For experiments in the presence of P_i, the solution above contained in addition 10 mM while the [Na_2CrP] was lowered to 31.0 mM to keep μ constant.

Tracking algorithm and length measurement

Fluorescence patterns were tracked frame by frame from 16 bit images with a region-based tracking algorithm (21). Briefly, in video data a single frame and its subsequent frame are called the ''template image'' and the ''search image'', respectively. In the first (template) image of the movie a ROI was set semiautomatically around the fluorescence patterns (''multiple windowing''). This initialization determines the coordinates of the center of each pattern in subpixel coordinates using a segmentation algorithm. Correspondence was then sought between ROIs of consecutive frames on the basis of a geometric transition (displacement, rotation, scaling) and a maximum likelihood estimation. Thereby, the minimal sum of squares of the differences (SSD) between the ROI transition of the template image and the reference ROI of the search image was sought while assuming normally distributed noise. The accuracy of the match was determined via noise analysis, and the maximum uncertainty was defined as three times the standard deviation of the positional estimate in image space, resulting in a confidence of 99.7% ($p < 0.01$). The displacement vector of the general geometric transition pointed toward the new position of the particular pattern in the search image. The rotation and scaling of a pattern from frame to frame were small and could be neglected. Subsequently, the search image was defined as the new template image, and its following image as the new search image, which completed the iterative computation. Finally, SL or hSL was defined as the Euclidean distance between the coordinates of the centers of two Z-patterns or between

an M-pattern and a Z-pattern, respectively. Accuracy in length was calculated from the accuracy of the positions by means of error propagation. The algorithm was written in C++ and MATLAB (The MathWorks, Natick, MA) and is fully automatic. An error analysis showed that the maximal error, i.e., the maximum of the difference between several analyses, is ±35 nm at high frame rate (low SNR) and ±10 nm at low frame rate (high SNR), determined by repetitive analysis and time-flipped videos. This systematic error originated in the initialization phase. At the end of the iterative step, the identification of ''old'' search and ''new'' template image is generally called ''template update''. It is a critical step in tracking algorithms because updating the template every frame might introduce systematic errors (''drift''). We assured that template drift is a minor problem by forward and backward (time-flipped) tracking. Hence, the presented method enabled us to determine initial SLs with 10–35 nm accuracy and to track the fluorescence patterns in reasonable time with subpixel resolution down to 0.05 pixels for displacements (~5 nm), depending on the SNR.

RESULTS

Specificity of binding of the antibodies to Z-lines and M-bands in myofibrils

Specificity of binding of antibodies was first investigated in myofibrillar samples under a high aperture fluorescence and phase contrast microscope with a 100× oil immersion objective (1.3 NA). Fig. 2, *A* and *B*, shows images of myofibrils from guinea pig ventricle and rabbit psoas which were stained as described in Materials and Methods for the mechanical experiments. The M-line signal was weaker than the Z-line signal. To selectively test the localization of the primary antibodies, immunostained myofibrils were prepared as for Fig. 2 *A* except that either only α-actinin Ab or only myomesin Ab was conjugated with the labeled IgG Fab fragment. Comparison with phase contrast images verified that myofibrils incubated with these α-actinin or myomesin Ab-containing complexes were exclusively labeled at their Z-lines or M-bands, respectively. Nonspecific binding of the Fab fragments could be excluded by incubating unlabeled myofibrillar suspensions with labeled Fab fragments for 10 min. These showed no fluorescence signal as unlabeled myofibrils, for which no autofluorescence could be detected. We therefore conclude that the staining procedure worked well with target-specific binding.

Fig. 3 shows stained myofibrils mounted in the apparatus. Combination of phase contrast and fluorescence microscopy allowed the colocalization of the fluorescence patches relative to the A-band and I-band pattern in phase contrast mode. By stretching the relaxed myofibril to the experimental SLs

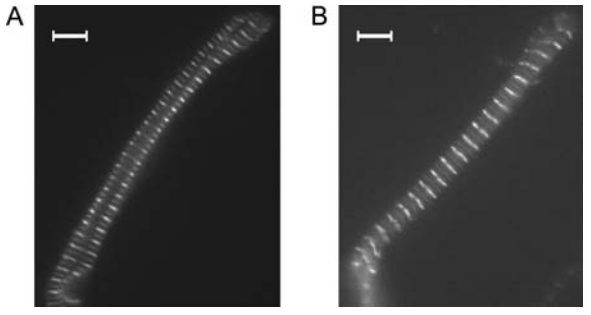

FIGURE 2 Epifluorescence images of α-actinin and myomesin double-stained cardiac and skeletal myofibrillar bundles prepared from guinea pig left ventricle (*A*) and rabbit psoas (*B*). Images were taken with a 100×/1.30 numerical aperture objective on a conventional inverted microscope setup (not in the mechanical apparatus). The repetitive fluorescence bands of stronger and weaker intensity refer to the α-actinin and myomesin Ab signals, respectively. Bars, 5 μm.

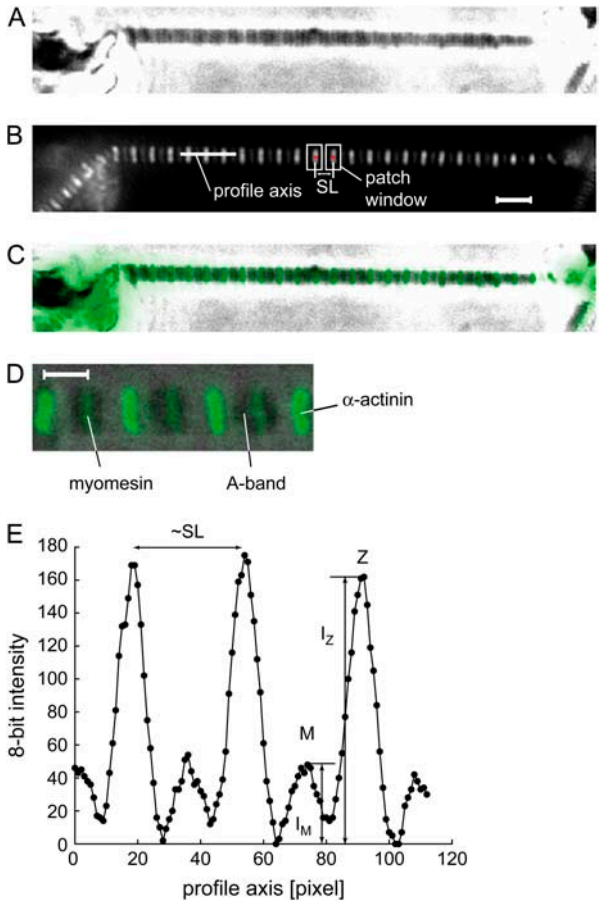

FIGURE 3 Micrographs of a cardiac myofibril mounted in the experimental apparatus for contraction experiments. The images were taken with the dry-type, long-distance objective. (*A*) Phase contrast light micrograph (enhanced). Mean SL was 2.4 μm. The typical structure of the sarcomeres revealed darker A-bands and lighter I-bands. (*B*) Same as in *A* but in fluorescence detection mode. Two patch windows (*rectangles*) around Z-line signals used for further image processing are indicated. Individual SL was calculated from the difference in coordinates of adjacent patch centers (*red crosses*). Bar, 5 μm. (*C*) Superposition of the phase contrast image in *A* with the fluorescence image in *B*. The Z-signals were localized between the A-bands, and the weak M-band signal was located in the middle of the A-band. (*D*) Overlay of a bright field image and a fluorescence image taken after the myofibril was stretched to mean SL 3.7 μm. A-bands are dark patterns with a low fluorescent signal of myomesin in the center. Strong α-actinin signals are narrow patches at the Z-line and do not trespass the I-band. Bar, 2 μm. (*E*) Intensity profile (8-bit sampling; maximum = 255) of the fluorescent patterns along the line profile axis indicated in *B*. Large peaks of the α-actinin fluorescence (intensities, I_Z) dominated the smaller peaks of the myomesin fluorescence (intensities, I_M).

of ~2.4 μm, it could be shown that anti-α-actinin binding corresponds with the center of the I-band in phase contrast and anti-myomesin fluorescence is localized in the center of the A-band. Stretching myofibrils to ~3.5 μm (Fig. 2 *C*) shows that anti-α-actinin binding selectively localizes at the Z-line and not in the I-band, which excludes nonspecific binding of the α-actinin Ab to actin. Images acquired with the dry-type objective produced a peak intensity ratio of ~1:3 between M-band and Z-line signal. This difference in fluorescent light intensity might be explained by the small presence of epitopes in the M-band compared to the dense network of α-actinin in the Z-line. However, we occasionally observed higher intensity ratios (up to 1:1.5) between M-band and Z-line signals in very thin (~1 μm in diameter), single myofibrils. As prolongation of incubation time from 10 min to 30 min did not increase the signal intensities of the fluorescent antibody complexes in thinner and thicker myofibrillar bundles (not shown), this might suggest that even under saturating incubation times and the thin myofibrillar bundles of a few micrometers diameter used in our study, the myomesin antibody complex might not have complete access to all binding sites as its free diffusion into the H-zone could be obstructed by its own binding, as suggested by the study of Kraft and co-workers (25).

Distribution of resting SL

SLs at rest exhibited variability of up to 300 nm. Histograms in Fig. 4 show the distribution of the difference between individual SL and mean SL along either cardiac (*left*) or psoas (*right*) myofibrils. More precisely, we calculated SL_j – mean(SL) for every sarcomere j in different myofibrils and collected data of 100 cardiac and 41 psoas sarcomeres in total. By assuming a Gaussian distribution, the standard deviation of these differences was calculated. Resting SL in cardiac myofibrils was more variable (SD = 62 nm) than in psoas myofibrils (SD = 40 nm). The variability found in psoas myofibrils was still higher than the accuracy limit for the lowest SNR images (35 nm). Furthermore, we tested whether SL is correlated to the sarcomere position (number) in the myofibril, and found only one significant correlation out of eight cardiac myofibrils, and none out of three psoas myofibrils. Thus, variability in SL was distributed only in one case in a gradient manner, but in all other cases rather randomly along the myofibril. Therefore, variability in resting SL results rather from randomly distributed variability of intrinsic mechanical or structural properties of passive series elastic elements in different sarcomeres than from manipulations of myofibrils during preparation or mounting into the setup.

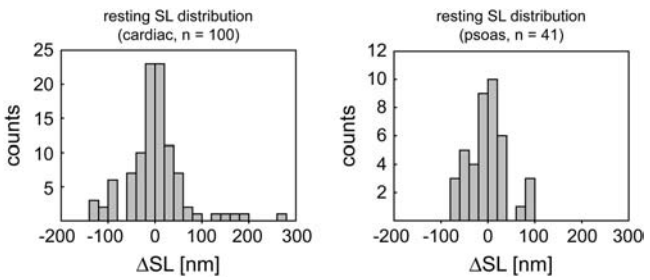

FIGURE 4 Resting SL variability illustrated by histograms of the difference of individual SL to mean SL in each myofibril, gathered from eight cardiac (*left*) and three psoas myofibrils (*right*), giving a total number of analyzed sarcomeres of $n = 100$ and $n = 41$, respectively. Note that the accuracy of initial SL is 14–35 nm, depending on the SNR.

Functionality of the immunofluorescently labeled myofibrils

After mounting, labeled cardiac and psoas myofibrils had slack SLs of 2.01 ± 0.04 μm and 2.34 ± 0.04 μm, respectively, showing that the staining procedure did not induce contraction of myofibrils. The average active force per cross sectional area (mean ± SE) developed by 15 cardiac myofibrils and 12 labeled psoas was 141 ± 26 nN/μm^2 and 186 ± 25 nN/μm^2, respectively. Active force of labeled cardiac myofibrils is therefore slightly, but not significantly, lower than previously reported for unlabeled cardiac myofibrils (18). Table 1 shows a summary of the force kinetic parameters of the myofibrils from which sarcomere dynamics were either quantitatively analyzed (see Results) or videos visually examined (see Discussion). The rate constants of Ca^{2+}-induced force development (k_{ACT}) and of the initial, slow linear force decline after Ca^{2+} removal (k_{LIN}) were not significantly different from previously reported values for cardiac myofibrils (18). This indicates that the immunostaining did not alter turnover kinetics of cross-bridges. Furthermore, compared to the previous results in unlabeled cardiac myofibrils, no significant differences were found in the duration of the initial, slow, linear force decline t_{LIN} and the rate constant k_{REL} of the subsequent, rapid exponential force decay. As t_{LIN} is determined by the onset and k_{REL} by the overall speed and extent of sarcomere ''give'' during relaxation, this is indirect evidence that the immunofluorescence-labeling procedure did not cause significant effects on sarcomere dynamics during relaxation. The values of the kinetic parameters of labeled psoas myofibrils were not significantly different from those of unlabeled controls prepared

TABLE 1 Force kinetic parameters of immunofluorescently labeled myofibrils

	k_{ACT} [s^{-1}]	k_{LIN} [s^{-1}]	t_{LIN} [ms]	k_{REL} [s^{-1}]
Guinea pig, cardiac	1.51 ± 0.15	0.52 ± 0.08	123 ± 19	9.2 ± 1.5
Rabbit psoas, labeled	5.0 ± 0.4	1.6 ± 0.2	91 ± 4	23 ± 3
Rabbit psoas, unlabeled	5.5 ± 0.5	1.5 ± 0.1	86 ± 9	21 ± 4

Values represent (mean ± SE) of 15 labeled cardiac, 12 labeled psoas, and 6 unlabeled psoas myofibrils, respectively.

from the same psoas muscles (Table 1). The values of labeled and unlabeled psoas myofibrils obtained here at 10°C are in between those reported by Tesi and co-workers for unlabeled psoas myofibrils at 5°C and 15°C (26).

Sarcomere dynamics in cardiac myofibrils

To assure that the mean SL during the contraction was optimal, we compensated the ''give'' of the series viscoelasticity during activation by slightly stretching relaxed sarcomeres before activation. Fig. 5 *B* shows exemplary data of SLs and corresponding force transient upon switching from pCa 7.5 to pCa 4.5 and back to pCa 7.5 from a cardiac myofibril under standard conditions. The myofibrillar segment consisted of 11 sarcomeres, of which one near the cantilever showed practically no active shortening and presumably operated as pure passive force transmitter (sarcomere 11) and

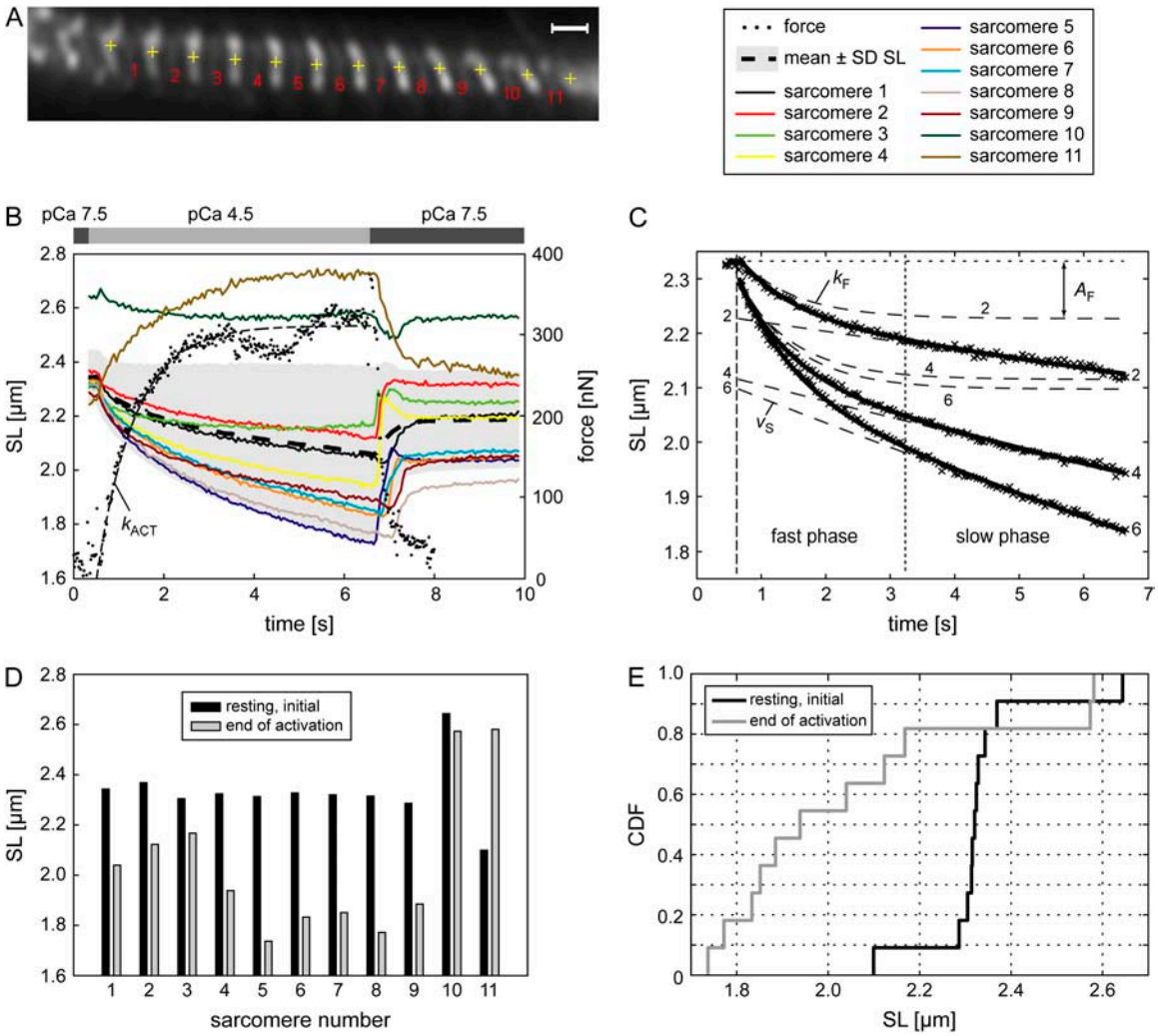

FIGURE 5 Force kinetics and sarcomere dynamics of a cardiac myofibril during contraction. (*A*) Fluorescence light micrograph of the cardiac myofibril during contraction. Each cross indicates the center fitted to the Z-line pattern. Sarcomeres involved in the analysis are numbered (Nos. 1–11). Bar, 2 μm. (*B*) SL traces (*colored lines*) and force transient (*dotted*) during the whole experiment. The numbering of sarcomeres in the legend corresponds to the numbers in *A*. Before activation, initial SL of the majority of sarcomeres (Nos. 10 and 11 excluded) ranged from 2.29 μm to 2.37 μm with a mean of 2.32 μm. Subsequent shortening of the majority of sarcomeres due to activation was nonuniform. Sarcomere 11 was presumably not operating actively but transmitting force passively. The ripple after the rise in force in the force signal is an artifact. The dashed line superimposed on the force signal is an exponential fit with a rate constant k_{ACT} of 1.5 s^{-1}. The mean SL of all sarcomeres is represented by the dashed line, and the increasing standard deviation of SL during contraction is shown by the light gray envelope. Temporal resolution, 50 ms. Accuracy of lengths, 10 nm. Accuracy of initial SL, 14 nm. (*C*) Analysis of the shortening dynamics of sarcomeres 2, 4, and 6 from *B*. These sarcomeres had similar initial length but exhibited different shortening dynamics. The SL traces were fitted with a biexponential function (*outlined*). The fast and slow components are plotted separately and numbered for every sarcomere involved (*dashed*). (*D*) Distribution of initial resting SL (*black*) and SL at the end of activation (*gray*). Sarcomere numbers correspond to the legend shown on top. Correlation of sarcomere number with SL was not significant in both resting ($r = 0.05$) and activated ($r = 0.35$) sarcomeres. (*E*) CDF of the SL distribution shown in *D*. The distribution of lengths in contracting sarcomeres (*gray*) is too flat to fit the CDF of a normal distribution, whereas the CDF of resting SL (*black*) indicates similarity to a normal distribution.

another that shortened only a little while being slightly overstretched (sarcomere 10). Mean initial SL before activation was $L_0 = 2.34$ μm (all sarcomeres included). Individual initial SL of the majority (sarcomeres 10 and 11 excluded) varied between 2.29 μm and 2.37 μm with a mean of 2.32 μm. More importantly, SL changes during force rise did appear in a nonuniform manner, with some sarcomeres shortening faster than others and some being almost isometric at the end of the contraction. The accuracy of SL tracking was 7–10 nm during the whole time course. The series compliance of this cantilever (0.12 μm at 300 nN) and the glued ends of the myofibril, and mainly the sarcomere(s) being too close to the cantilever and tungsten needle to be tracked, were responsible for the overall shortening of the myofibril during contraction, indicated by the mean SL trace.

In Fig. 5 *C* the length traces of three different sarcomeres with almost the same initial length (±20 nm) were fitted using a biphasic function. The rate constants, k_F, of the initial, rapid, exponential shortening phase which occurs during the time of the force development is strikingly similar for all sarcomeres, but the amplitudes, A_F, of this phase are very different between the sarcomeres: $k_F = 1.087 \pm 0.098$ s^{-1}, $A_F = 179 \pm 52$ nm (mean ± SD of all sarcomere traces shown in Fig. 5 *B*). The velocity v_S of the subsequent slow phase of shortening, which persists at the force plateau, shows similar large variabilities as the amplitude A_F ($v_S = 32 \pm 18$ nm/s). Taken together, sarcomeres contract initially with similar rate constants (k_F) but different fast ($v_F \approx A_F \cdot k_F$) and slow ($v_S$) velocities during and after the force development, respectively, yielding shortening traces of similar shapes (kinetics) but different amplitudes (velocities). Moreover, Fig. 5 *D* shows that the variability in SL at the end of activation, just before relaxation, was much more pronounced than in initial resting SL. In both cases the correlation of SL and sarcomere number was not significant at the 5% level. The cumulative distribution function (CDF) suggests that SL variability at rest is presumably normally distributed (Fig. 5 *E*, *black curve*), whereas the distribution during contraction is complicated by the large dynamics, indicated by the nonsigmoidal, flat CDF (*gray curve*).

The relaxation was a nonuniform, but highly ordered process, which is indicated in Fig. 6 *A*. After rapid Ca^{2+} removal, the force decreased initially linearly until one sarcomere started to lengthen (''structural relaxation'') after a time t_{LIN} of 0.17 s. The subsequent lengthening of sarcomeres propagated sequentially from one sarcomere to the next. The corresponding rapid force decay was exponential with a rate constant k_{REL} of 8 s^{-1}. The average rate with which lengthening propagated in one direction along the myofibril was ~11 sarcomeres/s. The values of k_{REL} and the propagation rate were similar within the SD to those reported previously (18) for unstained cardiac myofibrils (11 ± 3 s^{-1}, 13 ± 3 sarcomeres/s). Short sarcomeres still existed during an active force below 10% of the initial force. We observed lengthening speeds in the range of 2.6–0.4 μm/s per sarcomere (1.10–0.17 L_0/s), whereby faster lengthening preferentially occurred at the beginning of the relaxation. In all contraction-relaxation experiments, the principal observations were a), relaxed sarcomeres started at randomly distributed SL (Fig. 4 and Fig. 5, *D* and *E*); b), contracting sarcomeres shortened nonuniformly, some almost being isometric at the end of the activation, whereas others were still shortening; c), after Ca^{2+} removal, pronounced active shortening did not occur (Fig. 6 *B*). However, from the current accuracy of our data, we cannot exclude active shortening of <10 nm per sarcomere; d), relaxation was highly nonuniform, exhibiting a sequential relaxation more pronounced in cardiac than in psoas myofibrils (e.g., see Fig. 9 *C*); and e), early lengthening sarcomeres transiently overstretched before shortening passively back to resting SL, which was not the case for the late lengthening sarcomeres. Especially, in the first activation-relaxation cycle, the final resting SLs were different from those before activation and after completing the first activation variability in resting SLs increased.

Fig. 7 demonstrates that without altering other chemical components (MgATP, MgADP, Ca^{2+}), the same cardiac myofibril as analyzed in Fig. 5 initiated spontaneous oscillatory contractions (SPOC) when 10 mM P_i was added to the solutions. Oscillations in SL frequently started spontaneously

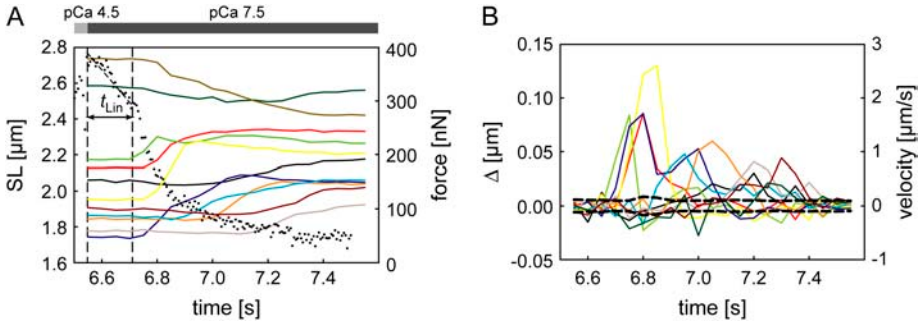

FIGURE 6 Sarcomere dynamics during relaxation of the cardiac myofibril. (*A*) Subset of force and SLs from Fig. 5 *B* during relaxation. After complete Ca^{2+} removal, the force decreased linearly during a period t_{LIN} in which SLs remained isometric. As soon as one sarcomere (sarcomere 3) started to lengthen, the force dropped exponentially. Lengthening of sarcomeres occurred one after another (average rate, ~11 sarcomeres/s). (*B*) Discrete derivative (displacement Δ and panel corresponding velocity) of the SL traces shown in panel *A*. The dashed traces represent the boundaries of uncertainty ($p = 0.01$) at each particular time point. During relaxation, negative length changes (shortening) were significantly detected only after pronounced positive length changes (lengthening). Thus, pronounced active shortening during relaxation was not detectable. Maximum lengthening speeds were 1.6–2.6 μm/s ≈ 0.7–1.1 L_0/s. Color code corresponds with the legend in Fig. 5. Temporal resolution, 50 ms.

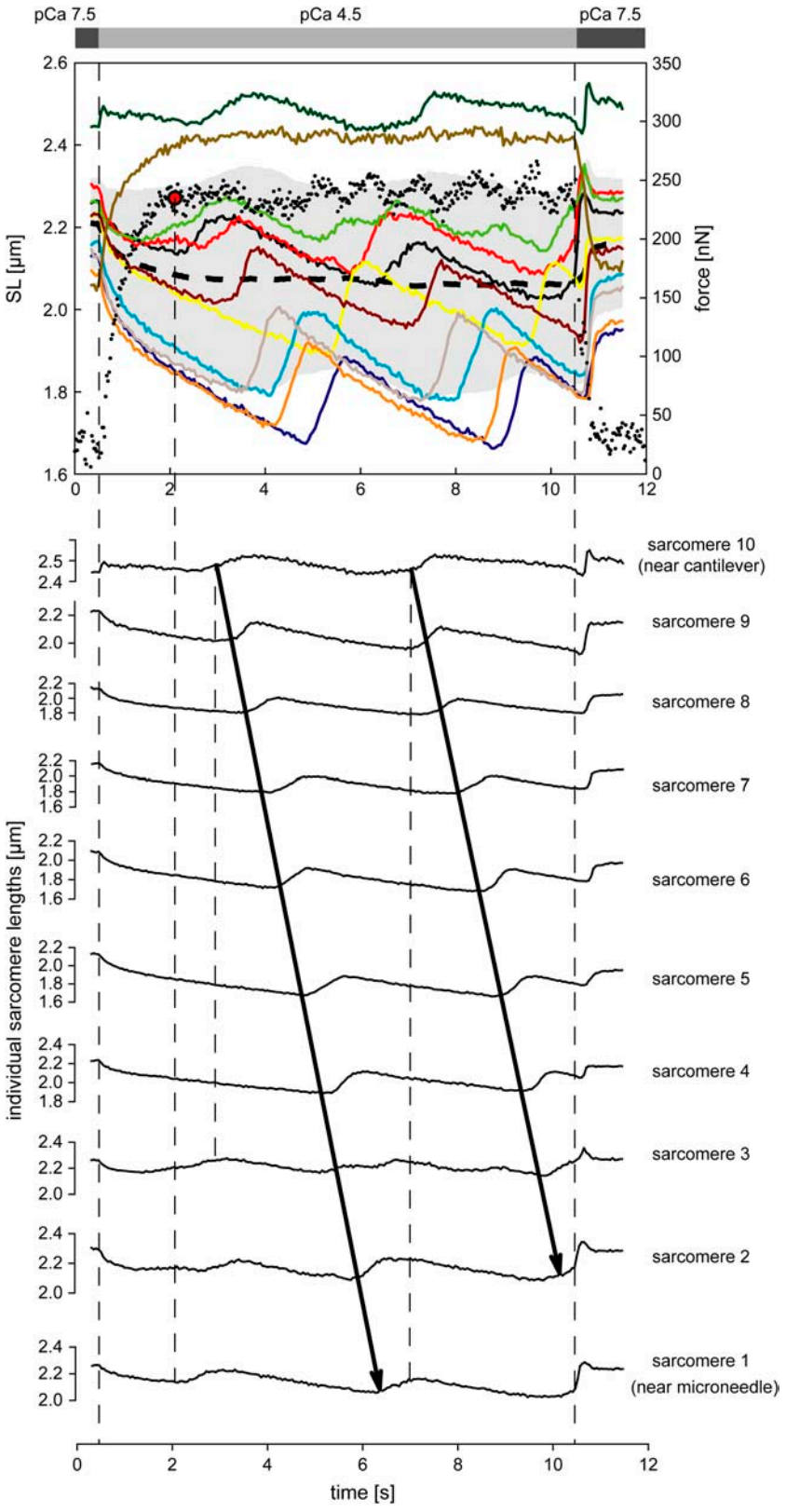

FIGURE 7 Spontaneous oscillation of SLs induced by 10 mM P_i (cardiac myofibril introduced in Fig. 5). Except for sarcomere 11 (passive), all others exhibited oscillatory fast lengthening (0.2 L_0/s mean) followed by slow shortening (0.03 L_0/s mean) during the force plateau. Lengthening occurred sequentially and propagated with a rate of ~2 sarcomeres/s along the myofibril (indicated by the *arrows* in the cascade plot on *bottom*). Lengthening started in sarcomeres 1–3 close to the motor when force approached its plateau and was then interrupted and newly initiated at the cantilever side. Reaching the motor side of the myofibril, the propagating length oscillations restarted at the cantilever side again. Structural relaxation started with the particular sarcomere (sarcomere 1) in which the propagation was located at and fast lengthening was just about to happen. Color code corresponds with the legend in Fig. 5.

at the time when force approached its plateau and then propagated in a highly organized manner along the myofibril as illustrated at the bottom of Fig. 7. The mean length, representing the total myofibrillar length, was almost constant during the sarcomeric oscillation, whereas the oscillatory amplitude in individual SL was 0.2 μm. During oscillation the lengthening velocity reached 0.2 L_0/s, whereas the shortening phase was with 0.03 L_0/s a magnitude slower. Lengthening spatially propagated with a rate of ~2 sarcomeres/s along the myofibril. Only one sarcomere at a time was lengthening, and the neighboring one started at about the time the previous one had stopped. During the plateau phase, the force signal exhibited a small amplitude oscillation with a frequency of ~0.7 Hz. The complex correlation between oscillations in force and individual SLs is best seen at the top of Fig. 7. Only sarcomere 11, close to the end of the cantilever which operated like a passive spring, shows some direct correlation in its small length oscillations with force oscillations. However, the force oscillation did neither clearly correlate with the length oscillations of single active sarcomeres nor did its frequency correlate with the frequency of the propagation across the whole preparation. One period of the force oscillation corresponded with fast lengthening of ~3 consecutive active sarcomeres. The beginning of force increase in the oscillatory force response corresponded with a transition from fast lengthening to isometric hold or shortening of one particular sarcomere. Hence, the force oscillations observed here reflect unpredictable small irregularities within the highly organized sequential process of SPOC. Importantly, this is a demonstration that the dynamics of sarcomeres cannot be deduced from analysis of force transients.

Half-sarcomere dynamics during relaxation in cardiac myofibrils

We investigated whether a sarcomere relaxes symmetrically during structural relaxation, i.e., whether both half-sarcomeres of an individual sarcomere lengthen synchronously, or whether one half-sarcomere relaxes after the other. To analyze this we introduced the term ''transfer time'', which we defined as the time period between the onset of lengthening of half-sarcomere j and the onset of lengthening of half-sarcomere $j + 1$. A transfer time significantly greater than zero implies sequential lengthening of the two consecutive half-sarcomeres, but for a transfer time converging to zero the two halves relax synchronously. Fig. 8 *A* shows hSL traces and the corresponding force trace of four consecutive half-sarcomeres in a cardiac myofibril. Structural relaxation started with hSL No. 1 close to the cantilever and propagated to hSL No. 2 by passing an M-band, and to hSL No. 3 by passing a Z-line, indicated by the arrows in Fig. 8 *A*. Qualitatively, this is a demonstration that half-sarcomeres relax sequentially in cardiac myofibrils. In three myofibrils we could track some M-band signals during the early and late relaxation phase. The hSL traces obtained from these three experiments were fitted with linear ramp functions (nonlinear fit using least-squares method, 6 ms sensitivity) to extract the transfer times (Fig. 8 *B*). By pooling these transfer times and defining the two sample groups ''Z-separated''

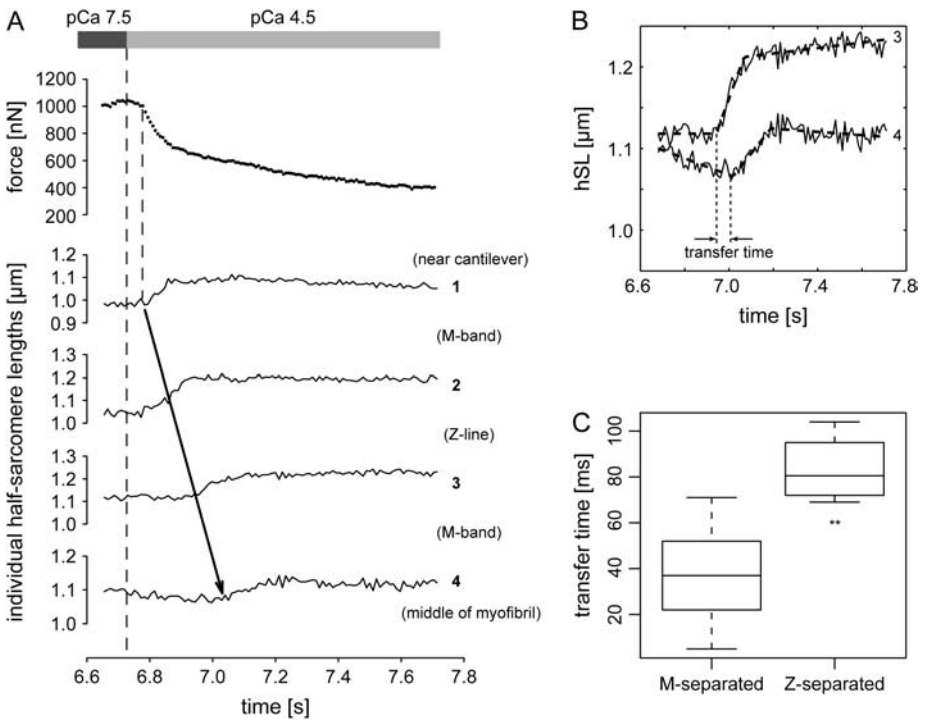

FIGURE 8 (*A*) Relaxation phase of a cardiac myofibril with corresponding force trace and lengths of four consecutive half-sarcomeres (numbered 1–4) near the cantilever where the structural relaxation started. During the initial, slow, linear force decay (t_{Lin} = 40 ms), all half-sarcomeres remained isometric until force dropped exponentially, mediated by the lengthening of the first half-sarcomere. Separation of half-sarcomeres by the Z-line or M-band is indicated in brackets. Accuracy of lengths, 17 nm. (*B*) shows length traces of No. 3 and 4 from *A* (*outlined*) with their fits (*dashed*) by ramp functions to illustrate the determination of the transfer time between consecutive half-sarcomeres. (*C*) Box plot of pooled and grouped data of transfer times between M-separated (*left*, $n = 6$) and Z-separated (*right*, $n = 4$) half-sarcomeres (median, quartiles, and extremes). The transfer time of M-separated half-sarcomeres was tested to be significantly different from zero ($p < 0.05$) and also significantly different (46 ms) from the transfer time of Z-separated half-sarcomeres ($p < 0.05$).

(transfer time of two hSL sharing a Z-line, $n = 4$) and ''M-separated'' (transfer time of two hSL sharing an M-band, $n = 6$), we performed two statistical tests with hypothesis H_0: a), the transfer time of M-separated hSL is zero, and b), the transfer times of M-separated and Z-separated hSL are identical. In case a we used the Wilcoxon signed rank test, and H_0 could be rejected ($p < 0.05$). H_0 in case b could be rejected using the Mann-Whitney U-test ($p < 0.05$). The Z-separated transfer times are 46 ms longer (estimate from statistical test, see Fig. 8 *C*). Thus, we show here with statistical significance that half-sarcomeres relax sequentially and that the transfer times of M-separated hSL are significantly shorter. From the mechanics of waves and wave propagation, we know that the mechanical coupling between two elementary masses is proportional to the group velocity of the wave and that the group velocity is inverse proportional to the transfer time. We conclude that the coupling between half-sarcomeres sharing the M-band is stronger than between those sharing the Z-line.

Half-sarcomere dynamics and A-band shift in psoas myofibrils

Psoas preparations are favorable regarding homogeneity in diameter and length and their regularity of the fluorescence signal. The clear signal of the fluorescence markers (Z-line, M-band) and the maintained undistorted structure allowed us to resolve half-sarcomere dynamics during the complete contraction-relaxation cycle. Fig. 9 *B* shows example data of individual hSL and force of a single psoas myofibril depicted in Fig. 9 *A*. Qualitatively, the dynamics during force rise are similar to that of whole cardiac sarcomeres shown earlier in this work. Thereby, some half-sarcomeres shortened more and faster than others, generating a nonuniform hSL distribution, some virtually on the plateau of their force-length relation (1.0–1.1 μm) and others on the ascending (<1.0 μm) or descending (>1.1 μm) limb. Early force rise is accompanied by fast shortening of all half-sarcomeres. Thereafter, although force reached its plateau, some half-sarcomeres still shorten, whereas others remain isometric or slightly lengthen within the accuracy. The increasing variance (*gray*) indicates progressively nonuniform hSL. This is a demonstration that a steady-state force does not imply steady state in half-sarcomeric dynamics.

In contrast to cardiac myofibrils, the propagation of lengthening during relaxation in psoas myofibrils was at least twice as fast (Fig. 9 *C*). Similar to the results shown above, the first half-sarcomere started to lengthen at the transition point from the linear to the exponential force decay. Within the limits of resolution, we could not detect a transfer time significantly different from zero. The sequential behavior of relaxing half-sarcomeres could not be determined for reasons of acquisition speed and accuracy. However, the faster structural relaxation observed in psoas indicates a stronger coupling between half-sarcomeres.

Interestingly, neighboring half-sarcomeres did not contract symmetrically. Fig. 10 shows length traces of neighboring (M-band separated, *B*) and adjacent (Z-line separated, *C*) half-sarcomeres for comparison. We could neither find left half-sarcomeres systematically shortening more than right ones or opposite, which we would have possibly rejected as systematic error from the optics, nor symmetry in general between neighboring half-sarcomeres. This finding enforces the idea that in terms of muscle mechanics the

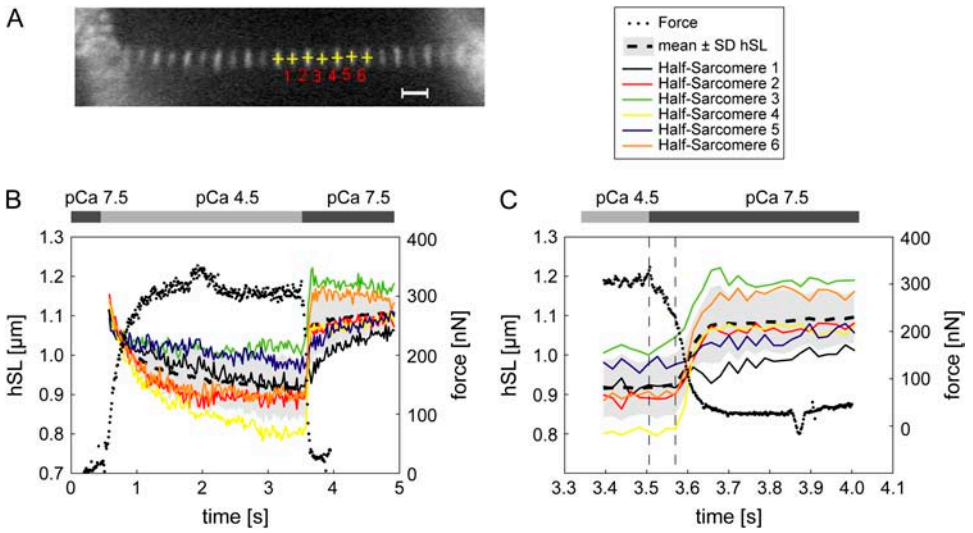

FIGURE 9 (*A*) Fluorescence light micrograph of a psoas myofibril. Strong fluorescence signals correspond to the Z-line, weaker patterns to the M-band. Half-sarcomeres involved in the analysis are numbered (Nos. 1–6). Myofibril width, 1.7 μm. SNRs: $SNR_M = 8$ (M-band), $SNR_Z = 13$ (Z-line). Bar, 2 μm. (*B*) Force and hSL traces during a contraction-relaxation cycle (switching from pCa 7.5 to 4.5 and back to pCa 7.5). The numbering of half-sarcomeres in the legend corresponds to the numbering in *A*. HSLs before activation ($t = 0.0$–0.5 s) could not be evaluated because of out-of-focus images. Variably shortening half-sarcomeres (8–28% L_0 shortening amplitude) coexisted and produced a maximal force of 320 nN (maximum tension, 141 nN/μm^2). The small ripples in the force signal are artifacts. (*C*) Detailed traces of the relaxation phase of half-sarcomeres introduced in *B*. The characteristic initial, linear force decline, during which half-sarcomeres remained isometric ($t_{LIN} = 60$ ms), was followed by a faster exponential decay. This was accompanied by fast half-sarcomeric lengthening, faster than in cardiac samples (half-sarcomeres 3, 4, and 6: lengthening speed 1.7–3.1 μm/s $\approx$ 1.5–2.7 L_0/s with mean $L_0 = 1.15$ μm). Temporal resolution, 22.8 ms. Accuracy of lengths, 20 nm. Accuracy of initial hSL, 35 nm.

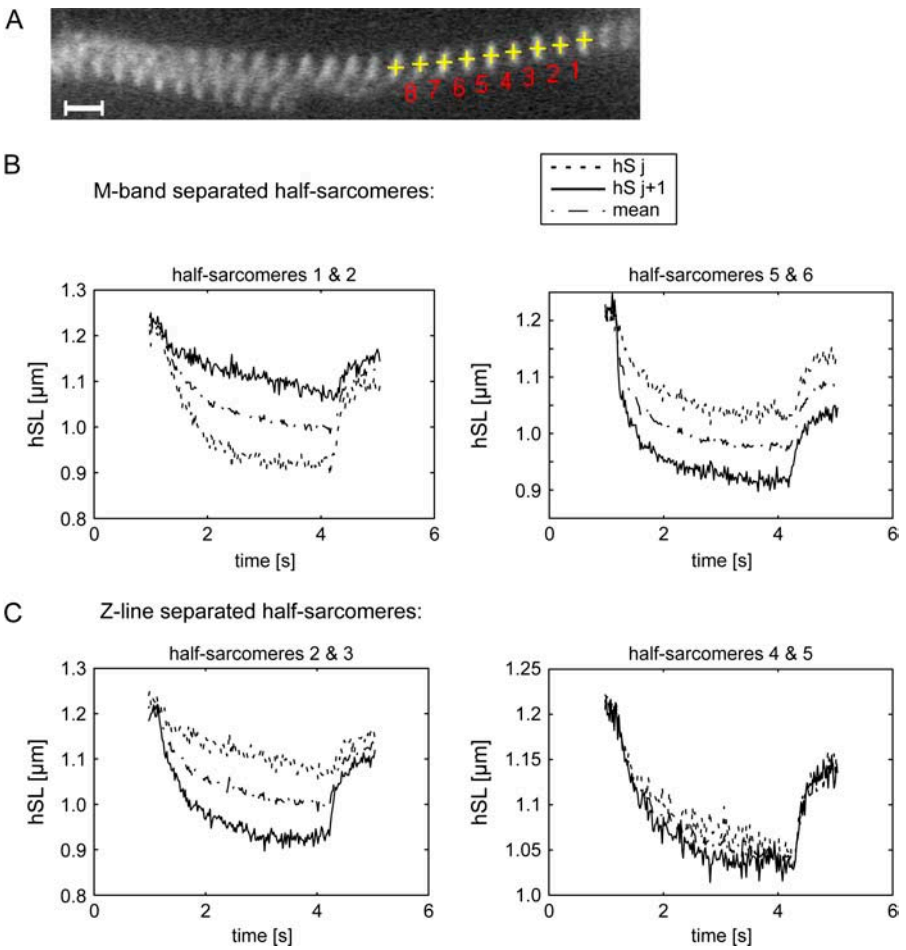

FIGURE 10 Examples of the dynamics of consecutive half-sarcomeres during isometric contraction of a psoas myofibril. Activation was induced at $t = 1.2$ s and relaxation at $t = 4.2$ s. (*A*) Fluorescence light micrograph of the relaxed psoas myofibril. Half-sarcomeres involved in the analysis are numbered (Nos. 1–8). Myofibril width, 1.4 μm. Bar, 2 μm. (*B*) Length traces of M-band separated half-sarcomeres, i.e., two neighboring half-sarcomeres sharing the M-band. (*C*) Length traces of Z-line separated half-sarcomeres, i.e., two adjacent half-sarcomeres sharing the Z-line. Plots depict hSL j (*dashed*, cantilever side) and hSL j+1 (*outlined*, motor side) with $j = 1,2,3\ldots$ as numbered in *A*. The dash-dotted traces represent the mean of the two hSL of the corresponding sarcomere, in *B* measured from Z-line to Z-line, and in *C* measured from M-band to M-band. Note that the dynamics of half-sarcomeres 4 and 5 was not significantly different. Accuracy of hSL, 16 nm.

half-sarcomere is the functional unit. From the asymmetric dynamics of the two halves in a sarcomere, we concluded that a displacement of the A-band (A-band shift) must have been present during contraction. In principle, assuming A-band symmetry relative to the M-band, the A-band shift is the distance between the center of the sarcomere (measured from one Z-line to the next) and the position of the M-band relative to the Z-lines (Fig. 11 *A*). The phenomenon of A-band shift is sometimes also termed ''instability of the thick filaments''. Here, we present unique data which indicate that such displacements can occur at the very early stage of the contraction, i.e., during the first couple of seconds, albeit not at large scales. Fig. 11 *B* shows the time-resolved displacement of a sarcomeric M-band of the myofibril introduced in Fig. 10 *A*. The M-band signal was shifted slowly toward the right Z-line during the contraction but quickly recovered its position as soon as the sarcomere relaxed. The measured shifts of 80–100 nm were significant with a maximum

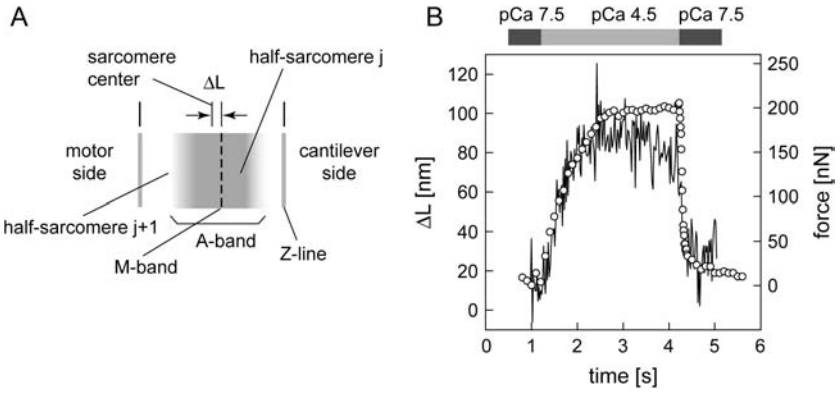

FIGURE 11 (*A*) Schematic representation of two half-sarcomeres forming a sarcomere, in which the A-band is displaced to the right. The displacement ΔL is defined as the distance between the sarcomere center (measured from Z-line to Z-line) and the position of the M-band. Positive displacement is in direction of the cantilever side. (*B*) Displacement trace (*outlined*) of the A-band, represented by the M-band signal, of the sarcomere comprising half-sarcomeres 1 and 2 in Fig. 10 *A*, and the corresponding force transient (*circles*). Accuracy of lengths, 15 nm.

uncertainty of 15 nm ($p < 0.01$). The dynamics of A-band shift during the early phase has a monoexponential shape which is strikingly similar to the kinetics of the Ca^{2+}-induced force development. Upon Ca^{2+} removal, the A-band changes its position similarly fast as observed for overall hSLs during relaxation.

DISCUSSION

Summary

The most important findings in individual sarcomere and half-sarcomere dynamics observed here in fixed-end myofibrils stained with (half)-sarcomere boundary markers are: a), Although active sarcomeres shorten rapidly during rise in tension upon Ca^{2+} activation and keep on shortening slowly during the tension plateau, the individual sarcomeres exhibit great variability in shortening velocities. b), The two halves of an individual sarcomere shorten with similar variability as two half-sarcomeres of different sarcomeres. The distinct shortening of the two halves in sarcomeres indicated A-band shifts which occur almost instantaneously in response to the force increase. c), In cardiac myofibrils, half sarcomeres relax individually, i.e., one after the other, whereby the mechanical coupling between half-sarcomeres separated by Z-lines is weaker than between those separated by M-bands. Our results provide for the first time direct experimental evidence for functional independent behavior of half-sarcomeres during contraction-relaxation cycles, proving their role as functional subunits of striated muscle. Our results further illustrate that the dynamics of individual sarcomeres or sarcomere populations cannot be predicted from force fluctuations alone. Complete understanding of force kinetics in multisegmental systems requires the investigation of their functional subunits.

Necessity, feasibility, and difficulties of the technique

Several studies have analyzed individual SLs or unitary length changes from fitting the center of mass in intensity profiles of either the intensity minima (18) or maxima (15–17) corresponding to the mean position of two adjacent I-bands and the A-band, respectively. Having shown with our method that half-sarcomeres in a myofibril are nonuniform in length and length change behavior, the center of mass of adjacent I-bands obtained in profile analysis of sarcomere patterns is not an appropriate estimate for the sarcomere boundaries, the Z-lines. At the short SLs under which skeletal and especially cardiac muscle physiologically work, unlabeled Z-lines are hardly to be resolved by conventional microscopy. Therefore, distinct lengths and distinct length changes of individual sarcomeres cannot be determined from bright field or phase contrast imaging. Also from fitting the A-band centers, one cannot distinguish A-band shifts from conventional, symmetrical filament sliding in both halves of the bilateral sarcomere by fitting the center of A-bands without having defined markers for the Z-line. In summary, without sarcomere or half-sarcomere boundary markers, individual SLs and hSLs and thereby sarcomere or half-sarcomere inhomogeneity cannot be determined exactly, and observed length changes and thus amount and velocity of filament sliding cannot be attributed to a certain half-sarcomere. Measuring sarcomere and hSLs by boundary markers is therefore compulsory when addressing questions about the degree of sarcomere homogeneity (17) or the positional stability of the thick filaments, i.e., A-band shifts (7,27). For our data shown here, collected in 10–50 ms time resolution, the tracking procedure allowed length change detection down to 5–10 nm or 15–20 nm for sarcomere or hSL, respectively. However, preliminary experiments (not shown) yielded spatial resolutions down to 2–3 nm if less time resolution (50–100 ms) was required, e.g., for the investigation of SL changes induced by slow stretch or releases.

We note, however, that the mechanical experiments with labeled myofibrils were difficult to perform. Selection and mounting of myofibrils and adjustment of the optics had to be performed under optical control by phase contrast and bright field imaging. This was accompanied by a prolonged light exposure, especially when we used the high aperture, water-immersion objective which was thermostated to guarantee the experimental temperature. Although we used high concentrations of antioxidants, we still found the stained myofibrils to be extremely sensitive. Photobleaching, i.e., loss of fluorescence signal was less a problem than phototoxicity, i.e., the loss in function indicated by reduced active myofibrillar force. In initial experiments we often had myofibrils mounted in the apparatus which looked perfect in shape, slack SL, and staining, but which did not generate force even in the first activation. Only the use of filters which completely blocked ultraviolet and excitation of the fluorescent label during mounting the myofibrils under phase contrast guaranteed their normal function. Still, the high run-down of myofibrillar force in consecutive activations under the fluorescent light excitation clearly indicated phototoxicity as a crucial factor which affects the functional integrity of the myofibrils. It is noteworthy that this run-down in active force was accompanied with decrease in amplitudes of SL changes but not with alterations in rate constants of force kinetics and sarcomere dynamics. A final difficulty was to analyze the video data of cardiac myofibrils. We preferentially used small bundles rather than single cardiac myofibrils since the single ones produce low fluorescence intensities and exhibited a great loss in force after the first activation. However, in the functionally stable, thicker (2–3 μm in diameter) cardiac bundles, the SL and especially the hSL signals (weak M-band signals) could often not be evaluated quantitatively when the fluorescence bands of myofibrils lying on top of each other in the optical axis became tilted and/or shifted during contraction. Nevertheless, visual

examination of many of such videos in slow motion helped us to qualitatively test our conclusions derived from the exemplary, quantitative data shown in the results.

Sarcomere dynamics and nonuniformity during contraction

Many different methods have been elaborated to measure the regular structure of the thousands of subcellular units, the sarcomeres, at least as an average by segment length (6,28) or striation (29,30) monitoring, and by diffraction techniques (9,31). However, irregularities in the network of sarcomeres in a contracting fiber have always been a difficulty to cope with. Consequently, several intact fiber studies dealing with sarcomere nonuniformity (inhomogeneity) during end-held contraction (10,13), relaxation (9,32), and stretch (28,33) have been performed. Apart from speculations on consequent predictions, e.g., ''force enhancement after stretch'' (28,33), little is known about effects of nonuniformity. It has been agreed that SL nonuniformity prevents interpretation on the molecular level (34). Our observations of sarcomere dynamics in a controlled environment rule out the possibility of $[Ca^{2+}]$ irregularities being the only reason for nonuniformity. This stresses a more fundamental cause, presumably lying in the contractile structures itself.

Here we demonstrate complete data sets of lengths and force from individual sarcomeres of a myofibril during an activation-relaxation cycle which shows that sarcomere nonuniformity develops already during the rise in force after Ca^{2+} activation when sarcomeres shorten with different velocities. The period of force rise is of high interest for muscle physiologists because its rate constant reveals cross-bridge turnover kinetics (35). We find here that shortening dynamics of individual active sarcomeres during the force rise can be described by an exponential with rate constant k_F. Compared to the high variability in shortening velocities, the values of k_F are very similar for all sarcomeres. This suggests that nonuniformity during force development results rather from different numbers of active cycling myosin heads than from different turnover kinetics of cross-bridges within individual (half-)sarcomeres. Assuming different intrinsic kinetic properties of cross-bridges within individual sarcomeres, one would expect that sarcomeres containing slowly cycling cross-bridges shorten with slower k_F or even become initially lengthened by sarcomeres containing faster cycling cross-bridges exhibiting a faster k_F. Thereafter, the former sarcomeres might shorten for longer times or with faster velocities (v_S) than the latter sarcomeres as the number of cross-bridges in the former sarcomeres can still increase whereas the number of cross-bridges in latter sarcomeres reached its maximum. However, considering the similar rate constants of SL changes reflected by k_F and the similar shapes of (half)-sarcomere transients in a myofibril, such a scenario seems unlikely. Interestingly, the values of k_F were 20–30% lower than those of the rate constant of the exponential force development k_{ACT} (see Fig. 5 *B*). Considering the well-known relationship of steady-state shortening velocity on load, this result clearly shows that one cannot derive presteady-state shortening velocities from the steady-state *F-v* relation. The hyperbolic inwards curvature of this relationship predicts that during force development the velocity of shortening should decrease more rapidly than the rate of force rise. This would result in higher and not in lower values of k_F compared to k_{ACT}. The finding that $k_F < k_{ACT}$ therefore indicates that active shortening is not an instantaneous consequence of force during force development. Slower presteady-state dynamics of SL changes compared to force kinetics are in line with the sequence of events proposed by current cross-bridge models in which the force generating step precedes the step determining active shortening velocity (36–38). Investigation of k_F and k_{ACT} under different $[Ca^{2+}]$, $[P_i]$, [ADP], and [ATP] could help to dissect the coupling between force generation and active shortening under presteady-state conditions. This would be important since in physiological twitch or systolic contractions, striated muscles perform these two fundamental functions under presteady-state conditions.

When force reached its plateau in our experiments, sarcomeres still exhibited nonuniform shortening behavior with a variability (SD) in the slow shortening rate v_S of ~1% L_0/s. Similar long-lasting, nonuniform sarcomere dynamics have been found during the isometric tetanus in intact frog fast skeletal fibers at 2°C (28). An examination of length changes recorded in different segments (involving ~250 sarcomeres) along the fiber (28, Fig. 8 therein) yields a lower SD of ~0.2–0.3% L_0/s. However, if we assume that the observed variability is statistically reduced by the square root of the number of sarcomeres per segment, the extrapolated variability of length changes per sarcomere in intact fibers would be 3–5% L_0/s and thus higher than obtained here in short cardiac myofibrils at 10°C. Since the maximum shortening velocity in fast frog muscle at 2°C is ~2 L_0/s (11), thus ~2.5-fold higher than in our cardiac myofibrils at 10°C (~0.8 L_0/s), it seems reasonable to assume that similar degrees of sarcomere nonuniformity as observed in myofibrils also exist in intact fibers.

It is well known that under certain requirements, sarcomeres perform so-called SPOC. SPOC has been found in different cardiac myofibrillar preparations under partial Ca^{2+} activation (Ca-SPOC) (39–41). Ishiwata and co-workers demonstrated that SPOC also occurs even in the absence of Ca^{2+} under high ratios of [ADP]/[ATP] (ADP-SPOC) (41–43) and in the absence of regulatory proteins (44) which indicates that the mechanism of SPOC is not based on oscillatory changes in the state of activation (44). They further demonstrated by detailed analysis of the dependence of SPOC on [ADP], $[P_i]$, $[Ca^{2+}]$, and pH that Ca-SPOC and ADP-SPOC share a common mechanism (41,42), confirming their original conclusion that the minimum requirement for both SPOC types is the coexistence of weakly bound

(AM.ADP.P_i) and force-generating cross-bridges (AM.ADP) at levels exceeding a certain threshold proportion (45). The new finding here of P_i-SPOC under maximum Ca^{2+} activation and physiological buffer at high [P_i] in cardiac myofibrils is in line with this minimum requirement definition (45) since P_i is known to decrease active force independently of regulation by lowering the fraction of strongly bound in favor of weakly bound cross-bridges (46). We note that within the accuracy achieved by the tracking algorithm we could not detect P_i-SPOC in psoas myofibrils in the presence of 10 mM and 20 mM P_i. Occurrence of P_i-SPOC in psoas myofibrils with amplitudes $\geq$40 nm/sarcomere and periods of $\geq$100 ms could be excluded (data not shown). This finding is most likely related to the difficulty to obtain the Ca-SPOC state in psoas fibers (41). Whether the absence of Ca-SPOC and P_i-SPOC in psoas muscle is only related to structural properties of skeletal sarcomeres or also to the myosin heavy chain isoform is not clear. Recently, it has been shown that ADP-SPOC, which is known to occur in both cardiac and fast skeletal muscle (41–43), has lower amplitudes in rat myocardium containing fast α-MHC than in other myocardia containing slow β-MHC (47).

We note, however, that the minimum requirement of coexisting cross-bridge states only accounts for the steady-state situation but cannot fully explain our findings under presteady-state conditions. We never observed SPOC to initiate during the rise in tension at force development although the distribution of cross-bridge states passes transiently the SPOC region during force development. Thus, to account for presteady-state situations we suggest that in addition to the distribution of cross-bridge states SPOC is critically dependent on the ratio of the instantaneous rates of cross-bridge detachment to cross-bridge attachment. It is prevented as long as the flux of cross-bridges to strongly bound states exceeds or compensates the one to weakly bound states.

Half-sarcomere dynamics and relaxation

From the structural point of view, the sarcomere bordered by its Z-lines is regarded to be the structural unit cell of striated muscles. From a mechanical point of view hSL changes are the proper measure for the amount of filament sliding between actin and myosin filaments, and A. F. Huxley described his cross-bridge model (14) implicitly for the half-sarcomere. Nevertheless, little is known about whether half-sarcomeres in striated muscles act dependently on or independently from their neighbor. A. F. Huxley demonstrated that a single half-sarcomere can be selectively electrically stimulated to contract independently from its neighbors (48). Ishiwata and colleagues (49) showed image sequences of myofibrils which exhibit examples of half-sarcomeres lengthening at different times during ADP-SPOC. However, to our knowledge so far no quantitative data have been available to statistically test the hypothetical role of half-sarcomeres as functional, independently behaving units.

Here, we provide high-resolution length data of contracting and relaxing half-sarcomeres, which prove that neighboring half-sarcomeres do not operate symmetrically. The relaxation phase, which has been reported earlier to occur sequentially in cardiac sarcomeres (18), shows sequential behavior also on the half-sarcomere level. Our analysis of transfer times indicates that half-sarcomere relaxation is transmitted more slowly over the actin filament–Z-discs than over the myofilament–M-band complex. The coupling strength, which is inversely proportional to the transfer time, is therefore higher in the myofilament–M-band complex. However, it is unlikely that the relaxation mechanism is based on a pure material wave. Rather, it involves cross-bridge turnover kinetics and transversal strains of filament structures perturbing the free energy landscape of the actomyosin cycle. In their past study, Stehle and co-workers (18) proposed several ideas to explain the sequential behavior of sarcomeres during relaxation. Based on our results, we reconsider the following mechanism for steps 2 and 3 mentioned there, which relates the initial lengthening of a (half-)sarcomere to the dynamic state of its neighbor (coupling mechanism): i), The load on the thin actin/thick myosin filaments in the lengthening half-sarcomere drops due to the reverse power stroke and detachment of cross-bridges, causing a slight increase in thin/thick filament spacing. The force decrease emerges in all half-sarcomeres (series connection) and can be measured externally. ii *a*), For Z-line-separated hSL: with diminishing load on the thin filaments lateral strain in the Z-line, a rather stiff structure with ''zigzag'' pattern connecting the thin filaments (50) occurs while this strain causes a small increase in the thin filament spacing on the adjacent half-sarcomere. ii *b*), For M-band-separated hSL: since M-band proteins link thick filaments to hinder them from longitudinal displacement, but are rather loose in lateral direction (51), the increase in thick filament spacing is largely transmitted to the neighboring half-sarcomeres. iii), This increase acts as a perturbation in the kinetics of the cross-bridge cycle in the neighboring half-sarcomere, shifting the strain-dependent potentials toward detachment and causing rapid detachment of the remaining attached cross-bridges by forward kinetics. We point out that a linear model of springs and dampers (representing compliance and viscoelasticity) is not able to account for an organized, sequential behavior and time delays in elongation; simple length change of one sarcomere cannot be the coupling mechanism to initiate shortening of its neighbor only, since all other members in a mechanical chain experience this length change and shorten as well. The new scheme involves a ''true'' coupling mechanism in which only the neighbor senses the dynamic state of a relaxing half-sarcomere. The time lag that generates the propagating relaxation is caused by the perturbed cross-bridge kinetics itself. It has been shown that cross-bridge kinetics in cardiac and skeletal muscle has different rates and timescales (52), with rabbit psoas having an almost five times faster kinetics, and might therefore cause slower transfer times from half-sarcomere

to half-sarcomere in cardiac compared to psoas myofibrils. Step ii of the coupling mechanism is an instantaneous mechanical event, but it determines the amount of perturbation. Thus, the time lag is determined by lateral strain *and* cross-bridge kinetics. One might therefore expect from this model that the transfer time for Z-separated half-sarcomeres is longer than for M-separated half-sarcomeres, as the lateral stiffness of the Z-structure is higher than in the M-band (53), leading to smaller lateral strains and therefore smaller perturbations. A rigorous mathematical model of the proposed mechanical and kinetic events has to be formulated to prove its correctness. Such modeling would also allow evaluating the necessary mechanical properties of the transverse structure to generate the perturbation.

A-band shift and stability

It has been suggested that effective contraction can be achieved only if all sarcomeres, and thus all half-sarcomeres, operate homogeneously on the plateau region of the force-length relationship but could be impaired or even damaged if SLs become progressively nonuniform (54). It is further suggested that a system of cytoskeletal proteins (e.g., titin, myomesin) counteracts this undesirable effect or at least prevents muscle from severe malfunctioning (27,55,56). However, the concept of stabilization, especially of the thick filaments in the sarcomere, is mainly based on speculation from structural studies and single molecule mechanics on titin (57,58) and myomesin (59), but has not been analyzed in dynamic situations. We show here that during short contractions of psoas myofibrils the A-band can move up to 100 nm toward its neighboring Z-line. We argue that a difference in active force production of both halves of the sarcomere is responsible for such displacements and all sources of passive force production are too small to prevent these shifts. At the corresponding hSL (from 0.9 to 1.0 μm), including A-band shift (0.1 μm), the passive elastic force of titin in the stretched half-sarcomere remains below slack force (passive force at slack length, $\sim$1.2 μm) (16). Also, it seems that the rather small velocity of stretch (0.08 μm/s) of these passive structures during A-band shift does not produce enough viscous force. Much larger displacements (up to 60% of maximum possible movement) have been shown by EM to occur during much longer contractions in whole fibers (7). A-bands and Z-lines in whole fibers are connected to each other by laterally linking proteins (e.g., desmin), possibly leading to slower or smaller displacements than in single myofibrils. However, we do not imply that the displacements shown above represent completely the physiological situation. In isolated myofibrils transverse connections between sarcomeres are absent and sarcomeres might therefore show more instability than would be present in a physiological situation. Here, we want to stress the impression that connectin (titin) filaments alone do not necessarily stabilize sarcomeres (A-bands), which in turn suggests the assumption of a tight transverse network of intermediate filaments playing the stabilizing role. Our data are good evidence that thick filament displacement can occur, even at hSLs $\sim$1.1 μm (plateau region), and allows first assumptions on stability criteria in isolated sarcomeres. It will encourage comparisons with studies on larger systems (several parallel myofibrils, whole fibers) to characterize mechanically the lateral components of stabilization.

Implications for the interpretation of force transients

This study of individual (half-)sarcomere dynamics shows that the interpretation of force transients in terms of cross-bridge kinetics is complicated by the inhomogeneous behavior of individual half-sarcomeres during both contraction and relaxation. From the fact that all half-sarcomeres generate the same force we conclude, by using the basic ideas of Huxley's 1957 cross-bridge formalism, that a), force is a result of the convolution of unequal dynamic processes while fulfilling the boundary conditions of overall length (60), b), cross-bridge turnover kinetics among individual half-sarcomeres varies greatly during contraction due to the nonuniform dynamics or intrinsic structural differences, and c), this variability has again fundamental consequences for the force production. Hence, cross-bridge turnover kinetics might not be directly identified with force kinetics but need to be related to the dynamics of each particular half-sarcomere, e.g., by a correction term for the dynamic state and incorporation of an intrinsic variability. In which particular situations this correction is either crucial or practically negligible has to be further investigated in the future. It is a challenging task to develop a model that will adopt current cross-bridge models for a small number of sarcomeres in a multisegmental system and to incorporate intrinsic variabilities and coupling mechanisms between half-sarcomeres to reproduce all the dynamic phenomena described here.

CONCLUSIONS

The findings from this study have raised a number of issues. First, the observed nonuniform sarcomere dynamics during force development suggests that the number of potential cross-bridges in each (half-)sarcomere is variable. Second, the sequential half-sarcomere dynamics during relaxation involves a mechanism with higher complexity than earlier suggested, including a role of transverse structures (Z-line and M-band). Third, A-band stability is not guaranteed in single myofibrils, suggesting that titin alone is unable to center thick filaments during contraction in the sarcomere at physiological lengths. Fourth, sarcomere-shortening transients and force transients during force development deliver different information on the kinetics. Simultaneous measurement of force production and filament sliding in a certain half-sarcomere could be a promising novel tool to study the

kinetics of transitions in the cross-bridge cycle that transform force to movement.

We are grateful to J. C. Perriard (ETH Zurich) for the kind gift of the myomesin antibody and I. Agarkova (ETH Zurich) for technical help in the early stage of the studies. We thank K. W. Ranatunga (Bristol) for helpful comments on the manuscript. We thank G. Danuser (The Scripps) for the disposal of the core algorithm of the tracking software.

This work was partly financed by the Deutsche Forschungsgemeinschaft (SFB612-A2 to R.S. and G.P.). I.A.T. was supported by the Barth Fond at ETH Zurich and R.S. by the Köln Fortune Fond at the Medical Faculty, University Cologne.

REFERENCES

1. Huxley, A. F., and R. Niedergerke. 1954. Structural changes in muscle during contraction. Interference microscopy of living muscle fibres. *Nature*. 173:971–973.
2. Huxley, H. E., and J. Hanson. 1954. Changes in the cross-striations of muscle during contraction and stretch and their structural interpretation. *Nature*. 173:973–976.
3. Edman, K. A., A. Mansson, and C. Caputo. 1997. The biphasic force-velocity relationship in frog muscle fibres and its evaluation in terms of cross-bridge function. *J. Physiol.* 503:141–156.
4. Brenner, B. 1991. Rapid dissociation and reassociation of actomyosin cross-bridges during force generation: a newly observed facet of cross-bridge action in muscle. *Proc. Natl. Acad. Sci. USA*. 88: 10490–10494.
5. Piazzesi, G., M. Reconditi, M. Linari, L. Lucii, Y. B. Sun, T. Narayanan, P. Boesecke, V. Lombardi, and M. Irving. 2002. Mechanism of force generation by myosin heads in skeletal muscle. *Nature*. 415:659–662.
6. Gordon, A. M., A. F. Huxley, and F. J. Julian. 1966. The variation in isometric tension with sarcomere length in vertebrate muscle fibres. *J. Physiol.* 184:170–192.
7. Horowits, R., and R. J. Podolsky. 1987. The positional stability of thick filaments in activated skeletal muscle depends on sarcomere length: evidence for the role of titin filaments. *J. Cell Biol.* 105: 2217–2223.
8. Horowits, R., and R. J. Podolsky. 1988. Thick filament movement and isometric tension in activated skeletal muscle. *Biophys. J.* 54:165–171.
9. Edman, K. A., and F. W. Flitney. 1982. Laser diffraction studies of sarcomere dynamics during 'isometric' relaxation in isolated muscle fibres of the frog. *J. Physiol.* 329:1–20.
10. Mutungi, G., and K. W. Ranatunga. 2000. Sarcomere length changes during end-held (isometric) contractions in intact mammalian (rat) fast and slow muscle fibres. *J. Muscle Res. Cell Motil.* 21:565–575.
11. Edman, K. A., and C. Reggiani. 1984. Length-tension-velocity relationships studied in short consecutive segments of intact muscle fibres of the frog. *Adv. Exp. Med. Biol.* 170:495–509.
12. Edman, K. A., and C. Reggiani. 1984. Redistribution of sarcomere length during isometric contraction of frog muscle fibres and its relation to tension creep. *J. Physiol.* 351:169–198.
13. Julian, F. J., and D. L. Morgan. 1979. Intersarcomere dynamics during fixed-end tetanic contractions of frog muscle fibres. *J. Physiol.* 293: 365–378.
14. Huxley, A. F. 1957. Muscle structure and theories of contraction. *Prog. Biophys. Mol. Biol.* 7:255–318.
15. Bartoo, M. L., V. I. Popov, L. A. Fearn, and G. H. Pollack. 1993. Active tension generation in isolated skeletal myofibrils. *J. Muscle Res. Cell Motil.* 14:498–510.
16. Linke, W. A., V. I. Popov, and G. H. Pollack. 1994. Passive and active tension in single cardiac myofibrils. *Biophys. J.* 67:782–792.
17. Rassier, D. E., W. Herzog, and G. H. Pollack. 2003. Dynamics of individual sarcomeres during and after stretch in activated single myofibrils. *Proc. R. Soc. Lond. B Biol. Sci.* 270:1735–1740.
18. Stehle, R., M. Krüger, and G. Pfitzer. 2002. Force kinetics and individual sarcomere dynamics in cardiac myofibrils after rapid Ca(2+) changes. *Biophys. J.* 83:2152–2161.
19. Littlefield, R., and V. M. Fowler. 2002. Measurement of thin filament lengths by distributed deconvolution analysis of fluorescence images. *Biophys. J.* 82:2548–2564.
20. Agarkova, I., D. Auerbach, E. Ehler, and J. C. Perriard. 2000. A novel marker for vertebrate embryonic heart, the EH-myomesin isoform. *J. Biol. Chem.* 275:10256–10264.
21. Danuser, G., P. T. Tran, and E. D. Salmon. 2000. Tracking differential interference contrast diffraction line images with nanometre sensitivity. *J. Microsc.* 198:34–53.
22. Inoue, S., and K. Spring. 1997. Video Microscopy. Plenum Press, New York.
23. Stehle, R., M. Krüger, P. Scherer, K. Brixius, R. H. Schwinger, and G. Pfitzer. 2002. Isometric force kinetics upon rapid activation and relaxation of mouse, guinea pig and human heart muscle studied on the subcellular myofibrillar level. *Basic Res. Cardiol.* 97(Suppl. 1):127–135.
24. Grove, B. K., V. Kurer, C. Lehner, T. C. Doetschman, J. C. Perriard, and H. M. Eppenberger. 1984. A new 185,000-dalton skeletal muscle protein detected by monoclonal antibodies. *J. Cell Biol.* 98:518–524.
25. Kraft, T., M. Messerli, B. Rothen-Rutishauser, J. C. Perriard, T. Wallimann, and B. Brenner. 1995. Equilibration and exchange of fluorescently labeled molecules in skinned skeletal muscle fibers visualized by confocal microscopy. *Biophys. J.* 69:1246–1258.
26. Tesi, C., N. Piroddi, F. Colomo, and C. Poggesi. 2002. Relaxation kinetics following sudden Ca(2+) reduction in single myofibrils from skeletal muscle. *Biophys. J.* 83:2142–2151.
27. Agarkova, I., E. Ehler, S. Lange, R. Schoenauer, and J. C. Perriard. 2003. M-band: a safeguard for sarcomere stability? *J. Muscle Res. Cell Motil.* 24:191–203.
28. Edman, K. A., G. Elzinga, and M. I. Noble. 1982. Residual force enhancement after stretch of contracting frog single muscle fibers. *J. Gen. Physiol.* 80:769–784.
29. Huxley, A. F., V. Lombardi, and L. D. Peachey. 1981. A system for fast recording of longitudinal displacement of a striated muscle fiber. *J. Physiol.* 317:P12–P13.
30. Bagni, M. A., G. Cecchi, F. Colomo, and C. Tesi. 1988. Plateau and descending limb of the sarcomere length-tension relation in short length-clamped segments of frog muscle fibres. *J. Physiol.* 401:581–595.
31. Rudel, R., and F. Zite-Ferenczy. 1979. Interpretation of light diffraction by cross-striated muscle as Bragg reflexion of light by the lattice of contractile proteins. *J. Physiol.* 290:317–330.
32. Edman, K. A. 1980. The role of non-uniform sarcomere behaviour during relaxation of striated muscle. *Eur. Heart J.* Suppl A:49–57.
33. Julian, F. J., and D. L. Morgan. 1979. The effect on tension of non-uniform distribution of length changes applied to frog muscle fibres. *J. Physiol.* 293:379–392.
34. Sugi, H., and T. Tsuchiya. 1998. Muscle mechanics I: intact single muscle fibres. *In* Current Methods in Muscle Physiology: Advantages, Problems and Limitations. H. Sugi, editor. Oxford University Press, Oxford/New York. 3–31.
35. Brenner, B., and E. Eisenberg. 1986. Rate of force generation in muscle: correlation with actomyosin ATPase activity in solution. *Proc. Natl. Acad. Sci. USA*. 83:3542–3546.
36. Eisenberg, E., and T. L. Hill. 1985. Muscle contraction and free energy transduction in biological systems. *Science*. 227:999–1006.
37. Hibberd, M. G., J. A. Dantzig, D. R. Trentham, and Y. E. Goldman. 1985. Phosphate release and force generation in skeletal muscle fibers. *Science*. 228:1317–1319.
38. Siemankowski, R. F., M. O. Wiseman, and H. D. White. 1985. ADP dissociation from actomyosin subfragment 1 is sufficiently slow to

limit the unloaded shortening velocity in vertebrate muscle. *Proc. Natl. Acad. Sci. USA.* 82:658–662.

39. Fabiato, A., and F. Fabiato. 1978. Myofilament-generated tension oscillations during partial calcium activation and activation dependence of the sarcomere length-tension relation of skinned cardiac cells. *J. Gen. Physiol.* 72:667–699.
40. Linke, W. A., M. L. Bartoo, and G. H. Pollack. 1993. Spontaneous sarcomeric oscillations at intermediate activation levels in single isolated cardiac myofibrils. *Circ. Res.* 73:724–734.
41. Fukuda, N., H. Fujita, T. Fujita, and S. Ishiwata. 1996. Spontaneous tension oscillation in skinned bovine cardiac muscle. *Pflugers Arch.* 433:1–8.
42. Fukuda, N., and S. Ishiwata. 1999. Effects of pH on spontaneous tension oscillation in skinned bovine cardiac muscle. *Pflugers Arch.* 438:125–132.
43. Anazawa, T., K. Yasuda, and S. Ishiwata. 1992. Spontaneous oscillation of tension and sarcomere length in skeletal myofibrils. Microscopic measurement and analysis. *Biophys. J.* 61:1099–1108.
44. Fujita, H., and S. Ishiwata. 1998. Spontaneous oscillatory contraction without regulatory proteins in actin filament-reconstituted fibers. *Biophys. J.* 75:1439–1445.
45. Ishiwata, S., and K. Yasuda. 1993. Mechanochemical coupling in spontaneous oscillatory contraction of muscle. *Phase Transit.* 45:105–136.
46. Millar, N. C., and E. Homsher. 1990. The effect of phosphate and calcium on force generation in glycerinated rabbit skeletal muscle fibers. A steady-state and transient kinetic study. *J. Biol. Chem.* 265: 20234–20240.
47. Sasaki, D., H. Fujita, N. Fukuda, S. Kurihara, and S. Ishiwata. 2005. Auto-oscillations of skinned myocardium correlating with heartbeat. *J. Muscle Res. Cell Motil.* 26:93–101.
48. Huxley, A. F., and R. W. Straub. 1958. Local activation and interfibrillar structures in striated muscle. *J. Physiol.* 143:40P–41P.
49. Ishiwata, S., N. Okamura, H. Shimizu, T. Anazawa, and K. Yasuda. 1991. Spontaneous oscillatory contraction (SPOC) of sarcomeres in skeletal muscle. *Adv. Biophys.* 27:227–235.
50. Luther, P. K. 1991. Three-dimensional reconstruction of a simple Z-band in fish muscle. *J. Cell Biol.* 113:1043–1055.
51. Lange, S., M. Himmel, D. Auerbach, I. Agarkova, K. Hayess, D. O. Furst, J. C. Perriard, and E. Ehler. 2005. Dimerisation of myomesin: implications for the structure of the sarcomeric M-band. *J. Mol. Biol.* 345:289–298.
52. Poggesi, C., C. Tesi, and R. Stehle. 2005. Sarcomeric determinants of striated muscle relaxation kinetics. *Pflugers Arch.* 449:505–517.
53. Yoshikawa, Y., T. Yasuike, A. Yagi, and T. Yamada. 1999. Transverse elasticity of myofibrils of rabbit skeletal muscle studied by atomic force microscopy. *Biochem. Biophys. Res. Commun.* 256:13–19.
54. Morgan, D. L. 1990. New insights into the behavior of muscle during active lengthening. *Biophys. J.* 57:209–221.
55. Tskhovrebova, L., and J. Trinick. 2003. Titin: properties and family relationships. *Nat. Rev. Mol. Cell Biol.* 4:679–689.
56. Linke, W. A., D. E. Rudy, T. Centner, M. Gautel, C. Witt, S. Labeit, and C. C. Gregorio. 1999. I-band titin in cardiac muscle is a three-element molecular spring and is critical for maintaining thin filament structure. *J. Cell Biol.* 146:631–644.
57. Wang, K., J. G. Forbes, and A. J. Jin. 2001. Single molecule measurements of titin elasticity. *Prog. Biophys. Mol. Biol.* 77:1–44.
58. Tskhovrebova, L., J. Trinick, J. A. Sleep, and R. M. Simmons. 1997. Elasticity and unfolding of single molecules of the giant muscle protein titin. *Nature.* 387:308–312.
59. Schoenauer, R., P. Bertoncini, G. Machaidze, U. Aebi, J. C. Perriard, M. Hegner, and I. Agarkova. 2005. Myomesin is a molecular spring with adaptable elasticity. *J. Mol. Biol.* 349:367–379.
60. Denoth, J., E. Stussi, G. Csucs, and G. Danuser. 2002. Single muscle fiber contraction is dictated by inter-sarcomere dynamics. *J. Theor. Biol.* 216:101–122.